Supplementary Information

Confinement-Induced Enhancement of Parallel Dielectric Permittivity: Super permittivity Under Extreme Confinement

Mohammad H. Motevaselian, and Narayana R. Aluru [1)]

Department of Mechanical Science and Engineering, University of Illinois at Urbana-Champaign, Urbana, Illinois, 61801, USA

[1)] Corresponding Author/E-mail: aluru@illinois.edu

S.1. MD computational details and forcefields

In MD simulations, equations of motion were integrated with the leap-frog algorithm with a time step of 1 fs. During the simulations, temperature is kept constant at 298 K using the Nosé-Hoover thermostat[1] with a 0.2 ps time constant. For the bulk simulations, all systems were initially equilibrated for 5 ns, followed by a 20 ns of production run in isothermal-isobaric (NPT) ensemble with a pressure of 1 bar using Parinello-Rahman barostat.[2] For the short-ranged interactions, the cutoff radius was set to 1.2 nm. Both energy and pressure tail corrections[3] have been applied to the standard 12-6 LJ potential for the bulk MD simulations. The long-range electrostatic interactions were calculated using the particle mesh Ewald (PME) summation[4] with the tinfoil boundary condition (infinite dielectric) and a fast Fourier transform (FFT) grid spacing of 0.12 nm. Periodic boundary conditions were applied in all the directions. In order to obtain enough statistics to calculate the bulk dielectric permittivity, trajectories of atoms were collected every 0.05 ps. For the confined fluid simulations, all simulations were performed in the canonical ensemble (NVT). For confined simulations, periodic boundary conditions were applied in all the directions with an extra vacuum of length at least $3H$ in the z direction. The long-range electrostatic interactions were modeled employing the Ewald algorithm adapted for slab geometry (Ewald3dc),[5] which excludes the long-ranged electrostatic contributions from the periodic image cells. The LJ length and energy scale parameters for carbon atoms are 0.3390 nm and 0.2334 kJ/mol, respectively. We modelled water by the extended simple point charge model (SPC/E) and used the SHAKE algorithm[6] to maintain the molecule rigidity. For methanol and dichloromethane, all parameters were adopted from the All-Atom Optimized Potential for Liquid Simulations (OPLS-AA) forcefield[7] with the exception of dichloromethane charges, which were modified for more accurate estimation of its dielectric constant.[8] Quantum, atomic and electronic polarizability

effects are neglected, therefore, the fluid models are considered to be non-polarizable. In order to determine the number of confined fluid particles, each channel was connected to a big reservoir equilibrated for 8ns at a temperature of 298 K and pressure of 1 bar, to allow for particle exchange in an NVT ensemble. During this process, the reservoir density was monitored to make sure that it is within 2% of the bulk density. The parallel dielectric permittivity profiles were calculated using the binning method. Figure S1 shows that coarse bin sizes of 0.1 nm and 0.05 nm fail to properly capture the variation of the parallel dielectric permittivity especially near the interface. On the other hand, a bin size of 0.001 nm is too fine and requires unnecessary long trajectories to reduce statistical noise. We found that $\Delta z = 0.01$ nm is the optimal bin size to capture the spatial variations of the parallel dielectric permittivity using 40 ns of trajectory averaged over a set of 8 MD simulations each with different initial velocities and positions and a total time of 40 ns.

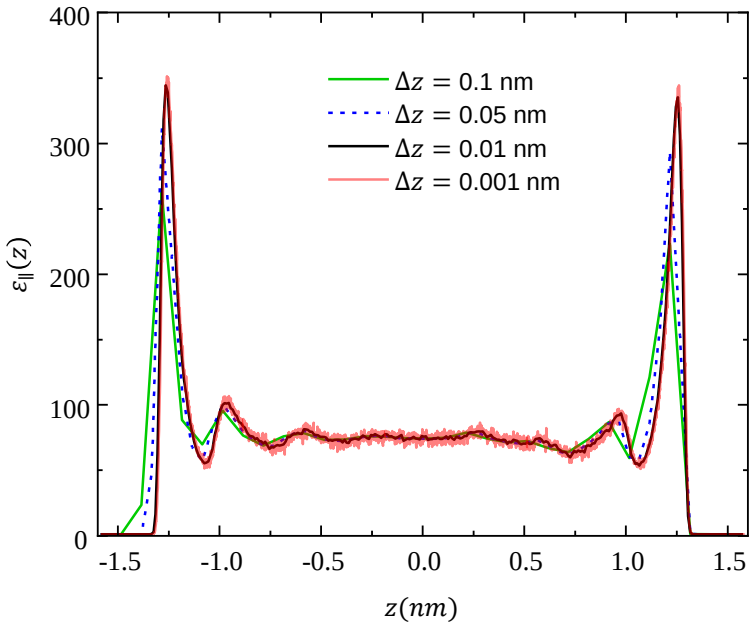

Figure S1. Parallel dielectric permittivity of water inside the 3.17 nm channel using various bin sizes, Δz.

S.2. Effect of higher-order moments on the parallel dielectric permittivity

To investigate the effect of higher-order multipole moments other than dipole, we have used the virtual cutting method[9] to calculate the parallel dielectric permittivity. The results in Figure S2 show almost identical profiles, indicating that the higher-order multipole moments beyond the dipole have negligible effect on the parallel dielectric permittivity for both protic and aprotic fluids.

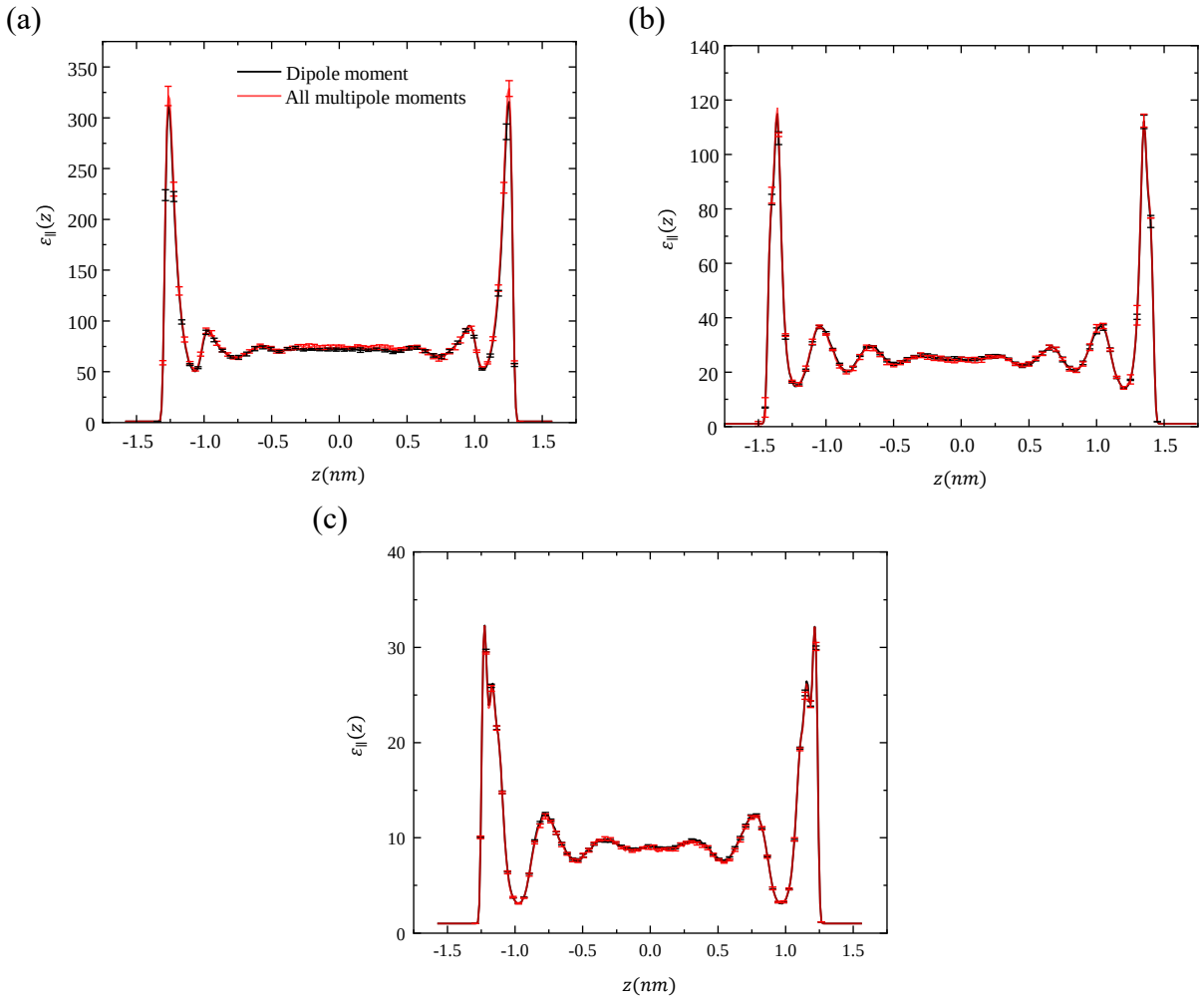

Figure S2. Parallel dielectric permittivity of confined fluids using molecular dipole moments (black color) and all multipole moments (red color): (a) water ($H = 3.17\ nm$), (b) methanol ($H = 3.5\ nm$), and (c) dichloromethane ($H = 3.15\ nm$)

S.3. Orientation profiles and angular distributions

To assess the alignment and orientation of the molecules next to the graphene surface, we have plotted the angular distribution of molecules in the IFL (Figure S3), $\cos\phi$, where ϕ is defined as an angle between the positive x axis and the fluid molecule dipole moment. We have also calculated the average cosine of dipole orientation (Figure S4), $\cos\theta\ (z)$, where θ is defined as an angle between the positive z axis and the fluid molecule dipole moment vector as shown in Figure S4.

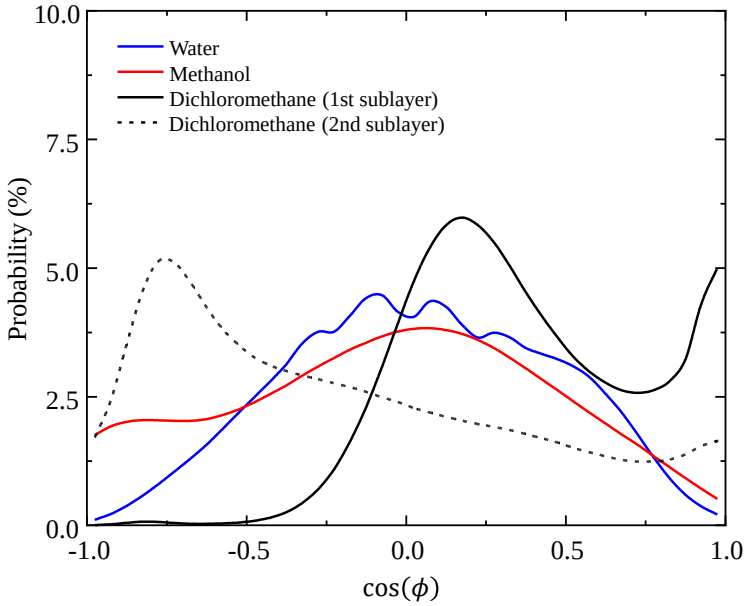

Figure S3. Histogram of the angle distribution of water, methanol, and dichloromethane molecules within the first density layer next to the graphene interface inside a large channel (well-defined bulk region in the middle of the channel) system.

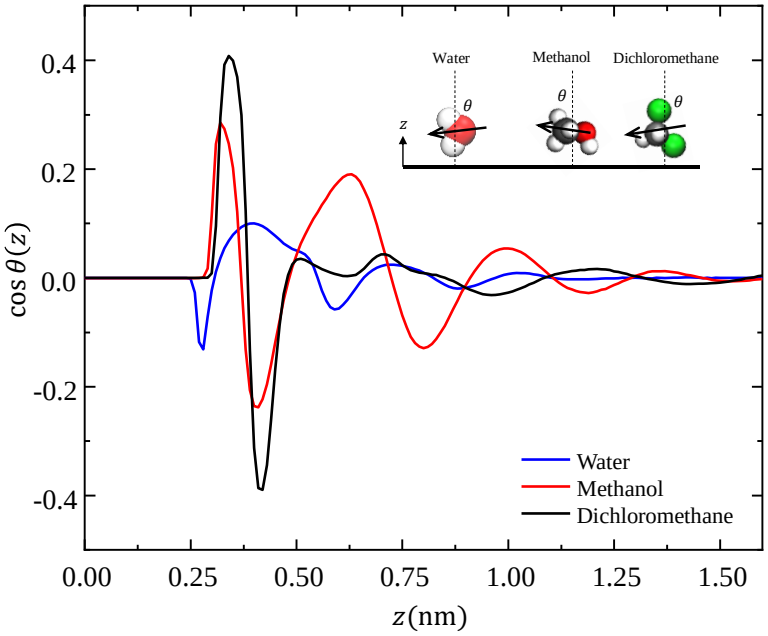

Figure S4. Dipolar orientation profiles of water, methanol, and dichloromethane inside the 3.17 nm, 3.5 nm, and 3.15 nm channels, respectively. Oxygen (O, red), hydrogen (H, white), carbon (C, grey), and chloride (Cl, green) atoms are shown.

By looking at Figures S3 and S4, we observe that the majority of water and methanol molecules tend to lie in the x-y plane next to the interface. In the case of dichloromethane, there are two preferred alignments of dipoles in the IFL region. Adjacent to the wall ($0 < z < 3.5$ Å), the molecules are aligned parallel to the surface, while the dipoles of the next layer are aligned perpendicular to the wall. This gives rise to the formation of two sublayers within the first density layer of dichloromethane next to graphene (Figure S5).

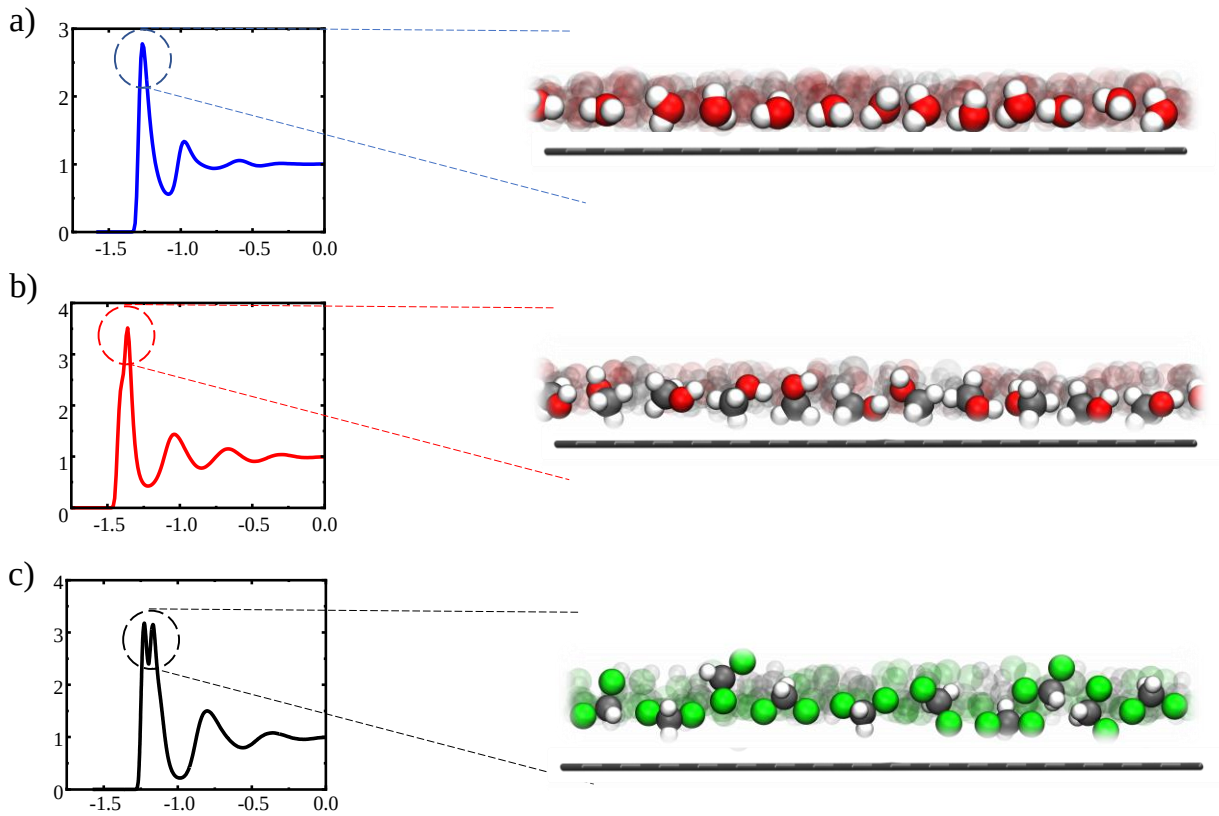

Figure S5. Density profiles (left) and molecular arrangement (right) of water (a), methanol (b), and dichloromethane (c) on the graphene surface. Oxygen (O, red), hydrogen (H, white), carbon (C, grey), and chloride (Cl, green) atoms are shown.

S.4. In- plane radial distribution function (RDF)

The in-plane RDF, $g(r_{\parallel})$, provides information on the planar (here, x-y plane) arrangement of molecules. It can be considered as an order parameter to identify ordering and possible phase transition close to an interface.[10] The RDFs are calculated in the slabs centered at the location of the maximum density with a thickness of 1 Å to avoid interference of atoms from the adjacent layers.[11] Figures S6(a-c) compare the in-plane RDFs in IFL and extreme confinement with the bulk radial distribution function. The IFL in-plane RDFs shows more structure compared to the

bulk indicating higher degree of ordering in the liquid. This becomes more evident in extreme confinement.

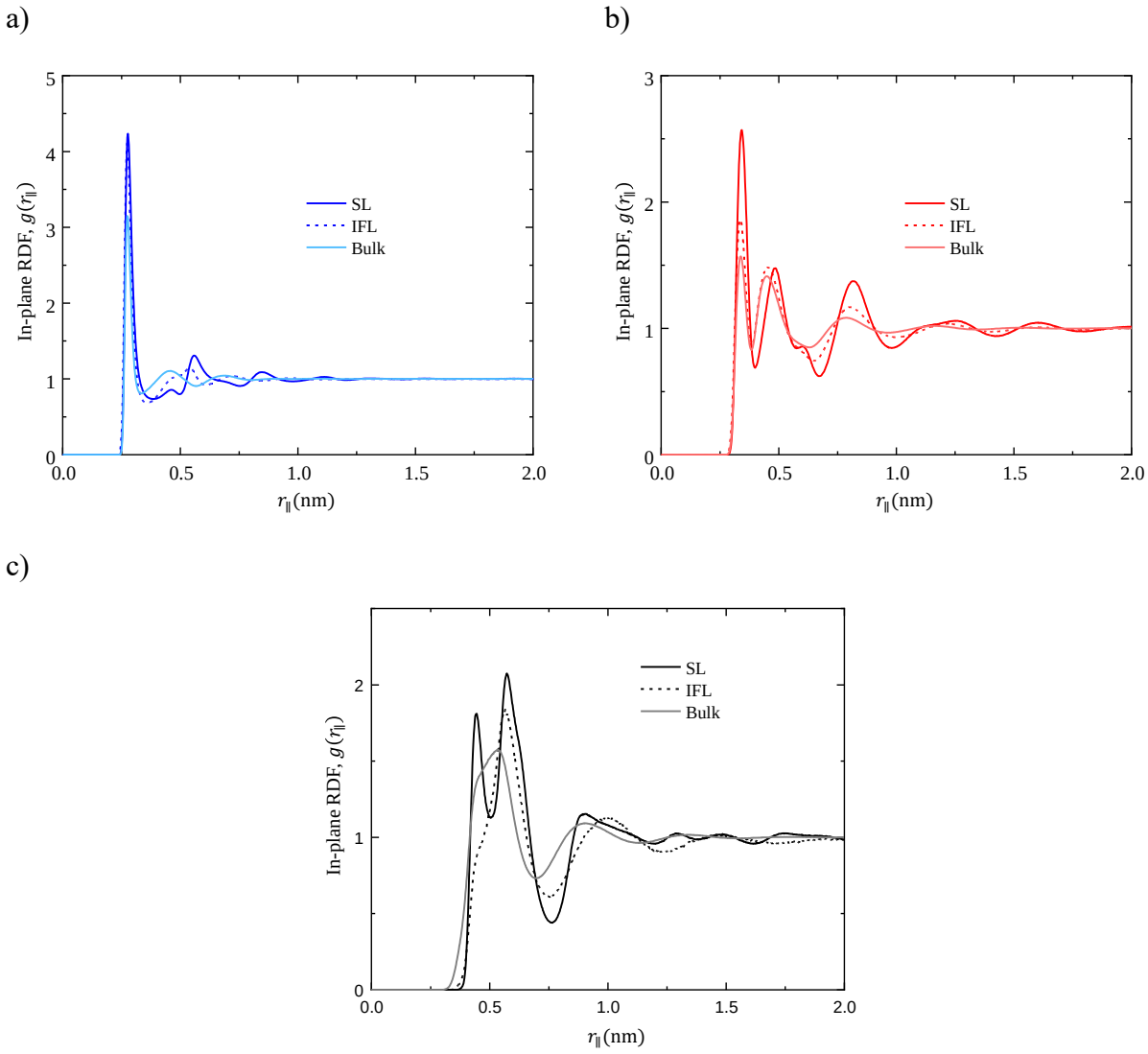

Figure S6. (a) Water in-plane RDF (b) methanol in-plane RDF and (c) dichloromethane in-plane RDF in the interfacial region, extreme confinement and bulk, respectively.

As illustrated in Figure S7, due to the degree of confinement, majority of the fluid molecules lie in the x-y plane. Depending on the fluid chemistry this planar arrangement can induce transition into higher-ordered structures or even a phase change. By looking at Figures S6(a) and S6(b), we observe that both water and methanol in-plane RDFs exhibit more pronounced peaks compared to the IFL indicating higher ordering in the first, second and third coordination shells. In the case of single layer dichloromethane (Figure S6(c)), we notice a higher ordering compared to the IFL, especially the emergence of a new peak located at $r = 4.4$ Å. To further analyze this, we obtained a 2D XY contour plot of the center-of-mass (COM) of dichloromethane molecules illustrated in Figure S8. It can be seen that under extreme confinement dichloromethane forms pentagon-like structures supporting the fact that extreme confinement can push liquid into higher-ordered structures with properties that are very different from not only bulk but also the interfacial region in the larger channels.

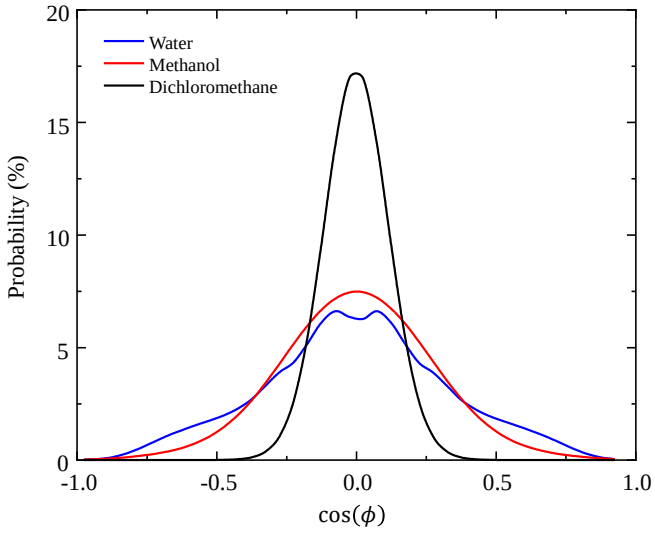

Figure S7. Histogram of the angle distribution of water, methanol, and dichloromethane in 0.634 nm, 0.7 nm, 0.7 nm channels, respectively.

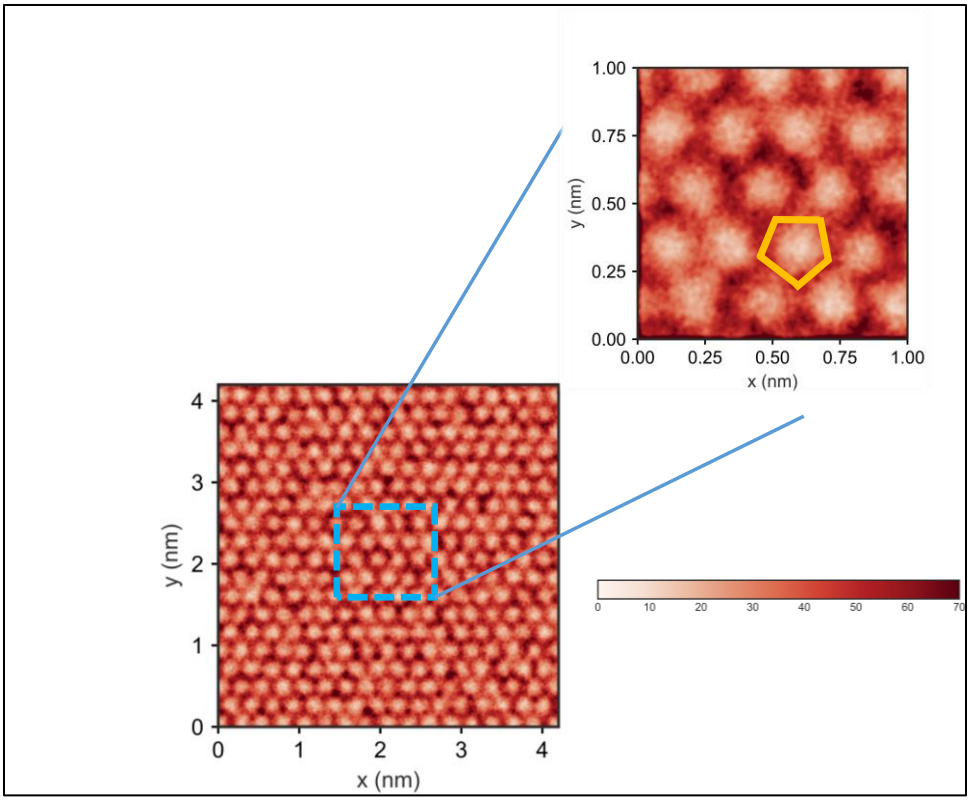

Figure S8. 2D XY contour plot of the COM of dichloromethane molecules inside a 0.7 nm slit-like graphene channel. The inset is the zoomed-in $1 \times 1\ nm^2$ contour plot showing a pentagon-like structure emerging *via* single layer arrangement of dichloromethane molecules.

References

(1) Nosé, S. A Unified Formulation of the Constant Temperature Molecular Dynamics Methods. *J. Chem. Phys.* **1984**, *81*, 511.

(2) Parrinello, M.; Rahman, A. Polymorphic Transitions in Single Crystals: A New Molecular Dynamics Method. *J. Appl. Phys.* **1981**, *52*, 7182–7190.

(3) Chialvo, A. A.; Cummings, P. T. Molecular-Based Modeling of Water and Aqueous Solutions at Supercritical Conditions. *Adv. Chem. Phys.* **1999**, *109*, 115–206.

(4) Darden, T.; York, D.; Pedersen, L. Particle Mesh Ewald: An N·log(N) Method for Ewald Sums in Large Systems. *J. Chem. Phys.* **1993**, *98*, 10089–10092.

(5) Yeh, I. C.; Berkowitz, M. L. Ewald Summation for Systems with Slab Geometry. *J. Chem. Phys.* **1999**, *111*, 3155–3162.

(6) Ryckaert, J. P.; Ciccotti, G.; Berendsen, H. J. C. Numerical Integration of the Cartesian Equations of Motion of a System with Constraints: Molecular Dynamics of *n*-Alkanes. *J. Comput. Phys.* **1977**, *23*, 327–341.

(7) Caleman, C.; Van Maaren, P. J.; Hong, M.; Hub, J. S.; Costa, L. T.; Van Der Spoel, D. Force Field Benchmark of Organic Liquids: Density, Enthalpy of Vaporization, Heat Capacities, Surface Tension, Isothermal Compressibility, Volumetric Expansion Coefficient, and Dielectric Constant. *J. Chem. Theory Comput.* **2012**, *8*, 61–74.

(8) Liu, Z.; Timmermann, J.; Reuter, K.; Scheurer, C. Benchmarks and Dielectric Constants for Reparametrized OPLS and Polarizable Force Field Models of Chlorinated Hydrocarbons. *J. Phys. Chem. B* **2018**, *122*, 770–779.

(9) Bonthuis, D. J.; Gekle, S.; Netz, R. R. Profile of the Static Permittivity Tensor of Water at Interfaces: Consequences for Capacitance, Hydration Interaction and Ion Adsorption. *Langmuir* **2012**, *28*, 7679–7694.

(10) Krott, L. B.; Barbosa, M. C. Anomalies in a Waterlike Model Confined between Plates. *J. Chem. Phys.* **2013**, *138*, 084505.

(11) Argyris, D.; Tummala, N. R.; Striolo, A.; Cole, D. R. Molecular Structure and Dynamics in Thin Water Films at the Silica and Graphite Surfaces. *J. Phys. Chem. C* **2008**, *112*, 13587–13599.